sustainable chemistry

MDPI

Article

One Step Synthesis of Ball-Milled $La_{0.6}Ca_{0.4}FeO_3$ Perovskite for CO_2 Conversion via Reverse Water–Gas Shift Chemical Looping

Hanzhong Shi, Fernanda Pimenta, Prabhsimran Singh, Venkat R. Bhethanabotla and John N. Kuhn *

Department of Chemical, Biological, and Materials Engineering, University of South Florida, Tampa, FL 33620, USA; hanzhongshi@usf.edu (H.S.); bhethana@usf.edu (V.R.B.)
* Correspondence: jnkuhn@usf.edu

Abstract

This study investigates the synthesis of $La_{0.6}Ca_{0.4}FeO_3$ (LCF) perovskite via a ball milling method for application in reverse water–gas shift chemical looping (RWGS-CL) for CO_2-to-CO conversion. Unlike conventional wet-chemical routes such as the Pechini method, the ball milling approach offers a solvent-free, scalable synthesis using low-cost metal oxide precursors (e.g., La_2O_3, CaO, Fe_2O_3). Structural analysis by XRD confirmed the successful formation of single-phase cubic perovskite, with no secondary phases when using oxide precursors. Crystallite size increased with calcination temperature, from 118.9 Å (no calcination) to 404.3 Å (1050 °C). BET analysis revealed a decrease in surface area from 2.5 m^2/g (no calcination) to 0.51 m^2/g (1050 °C), consistent with sintering at higher temperatures. TPR-H_2 and TPO-CO_2 studies revealed that non-calcined LCF possesses slightly enhanced redox properties, with oxygen vacancy formation and CO_2 reoxidation activity both at 500 °C. RWGS-CL experiments demonstrate that all LCF samples exhibit stable CO production (910–970 $\mu mol/g_{LCF}$) over multiple cycles at 500 °C, with comparable performance across calcination conditions. A cost and sensitivity analysis reveals that the ball milling method had lower synthesis costs by approximately 92% at the laboratory-scale and 88% at the industrial-scale compared to the Pechini method, highlighting its strong potential for large-scale perovskite production.

Keywords: perovskite oxides; ball-milling synthesis; reverse water–gas shift chemical looping; CO_2 to CO conversion; cost analysis

1. Introduction

The increasing availability of carbon dioxide (CO_2) has intensified the search for efficient and scalable CO_2 conversion technologies. A promising approach is the reverse water–gas shift chemical looping (RWGS-CL) process, which enables the conversion of CO_2 into carbon monoxide (CO), a valuable feedstock for synthetic fuels and chemicals [1]. RWGS-CL operates through a two-step redox cycle, where a metal oxide is first reduced by a reducing agent, typically hydrogen (H_2), followed by reoxidation with CO_2 to produce CO [2]. This process offers advantages over conventional RWGS reactions by avoiding the direct mixing of reactants, minimizing unwanted side reactions, and enhancing CO selectivity [3]. Perovskite-type oxides have emerged as attractive redox materials for RWGS-CL due to their ability to reversibly form and eliminate oxygen vacancies, facilitating CO_2 reduction under cyclic operating conditions [4,5].

Previous studies have demonstrated the efficacy of La-based perovskites, such as $La_{0.5}Ba_{0.5}FeO_3$ (LBF), $La_{0.75}Sr_{0.25}FeO_3$ (LSF), and $La_{0.6}Ca_{0.4}FeO_3$ (LCF), in enhancing

Check for updates

Academic Editor: Matthew Jones

Received: 25 June 2026
Accepted: 10 July 2026
Published: 16 July 2026

Copyright: © 2026 by the authors. Licensee MDPI, Basel, Switzerland. This article is an open access article distributed under the terms and conditions of the Creative Commons Attribution (CC BY) license.

CO yield and stability in RWGS-CL [6–8]. Supported perovskite, for example, silica-supported LBF (LBF/SiO_2) and silica-supported LSF (LSF/SiO_2), have been shown to improve CO_2 adsorption and increase carbonate formation, leading to enhanced reaction performance [9,10]. However, there remains a need to explore alternative perovskite compositions and synthesis methods to optimize material properties for long-term application.

Conventional synthesis methods for perovskite oxides typically involve solid-state reactions or sol–gel techniques [11,12]. The solid-state reaction method requires high-temperature calcination over long times, often leading to large particle sizes and limited control over defect structures [13–15]. Sol–gel based techniques, such as the Pechini method, provide better homogeneity but can involve complex processing steps (e.g., long stirring to transfer from solution to gel, and long-time/high-temperature calcination) and expensive precursors [16–18] and solvents. Thus, the sol–gel-based technique is difficult to scale up. In this study, we investigate $La_{0.6}Ca_{0.4}FeO_3$ (LCF) as a potential perovskite candidate for RWGS-CL. Unlike conventional solid-state synthesis, ball milling, a technique known to enhance material homogeneity, reduce particle size, and promote defect formation [19], is employed to achieve the targeted material. Ball milling introduces high-energy mechanical forces that improve mixing and induce structural modifications, which may lead to superior redox performance [20].

In this work, the direct synthesis and the effect of calcination temperature are examined for their impact on the physicochemical properties. By systematically evaluating the structural, redox, and catalytic properties of ball-milled LCF, we aim to elucidate its potential advantages over previously studied perovskite materials. This work provides new insights into the role of synthesis methods in optimizing perovskite performance for CO_2 conversion, advancing the development of efficient chemical looping systems.

2. Experimental Methods

2.1. Synthesis of $La_{0.6}Ca_{0.4}FeO_3$ (LCF) by Ball Milling

LCF was synthesized using a vertical planetary ball mill (XQM-8A; Tencan; Changsha, China). In this study, metal oxide precursors are prepared by calcination of metal nitrates, aiming to compare the resulting perovskite with that made from the same metal nitrate precursors. Similar perovskites would be formed by directly using metal oxide precursors. The precursor materials included La_2O_3 (derived from the calcination of $La(NO_3)_3{\cdot}6H_2O$, 800 °C, 4 h under air; Heeger Materials, ≥99.99%; Denver, CO, United States), CaO (HiMedia, ≥95%; Kennett Square, PA, United States), and Fe_2O_3 (obtained from the calcination of $Fe(NO_3)_3{\cdot}9H_2O$, 600 °C, 4 h under air; Sigma-Aldrich, ≥99.95%; St. Louis, MO, United States). Additionally, to compare the effects of different precursor materials, ball milling was performed separately using $La(NO_3)_3{\cdot}6H_2O$ and $Fe(NO_3)_3{\cdot}9H_2O$ to synthesize a control sample—$LaFeO_3$ (LF). The goal was to determine which precursor combination yields better performance in RWGS-CL. The ball milling process was conducted at 550 rpm for 8 h with a ball-to-powder ratio (BPR) of 10:1. Each milling batch produced approximately 100 g of the respective perovskite material. Following ball milling, the powder samples underwent different post-treatment conditions: no calcination (LCF-NC or LF-NC), calcination at 800 °C (LCF-800 or LF-800), 950 °C (LCF-950 or LF-950), or 1050 °C (LCF-1050 or LF-1050), each for 8 h.

2.2. Characterization Techniques

2.2.1. X-Ray Diffraction (XRD)

X-ray diffraction (XRD) was used to analyze the crystal structure of fresh and thermally processed samples. The measurements were performed using a Bruker X-ray Diffractometer

(Bruker; Massachusetts, UK) with Cu Kα radiation (λ = 0.154 nm) over a 2θ range of 20° to 80°, employing a step size of 0.0102° and a step time of 1.2 s/step.

2.2.2. N_2-Physisorption

N_2-physisorption was measured using a Quantachrome Autosorb IQ analyzer (Anton Paar; Graz, Austria) to determine the specific surface area. Samples were degassed at 300 °C, and N_2 adsorption–desorption isotherms at 77 K were collected (P/P_O = 0.05–0.3). Brunauer–Emmett–Teller (BET) surface area analysis was conducted to determine the surface area, and the Barrett–Joyner–Halenda (BJH) method was conducted to determine the porosity of the samples.

2.2.3. Scanning Electron Microscopy (SEM)

Scanning electron microscopy (SEM) was performed using a Hitachi SU70 scanning electron microscope (Hitachi; Santa Clara, CA, United States) to examine the morphology and particle size of the prepared LCF samples. Prior to analysis, the powder samples were dispersed onto conductive carbon tape mounted on aluminum SEM stubs. The samples were imaged under high vacuum at appropriate accelerating voltages and magnifications to obtain representative surface morphology images. Particle sizes were estimated from the SEM images by measuring multiple particles using image analysis software, and the average particle size was reported.

2.2.4. Redox Properties Testing

A lab-scale microreactor system (custom-built) was used to conduct temperature-programmed and four-cycle RWGS-CL experiments. Approximately 100 mg of the sample was placed between glass wool plugs in a quartz U-tube reactor, heated by a furnace. Gas flow was regulated using mass flow controllers (Alicat; Tucson, AZ, United States), with He, H_2, and CO_2 (Airgas, purity $\geq$ 99.99%) as feed gases. The reactor effluent was analyzed using a mass spectrometer (MS; MKS Cirrus 3; Andover, MA, USA).

For temperature-programmed reduction under hydrogen (TPR-H_2), approximately 100 mg of the sample was placed between glass wool plugs in a quartz U-tube reactor. The reactor was heated from room temperature to 800 °C at a rate of 10 °C/min under a 10% H_2/He gas flow (50 sccm).

For temperature-programmed oxidation with CO_2 (TPO-CO_2), approximately 100 mg of the sample was placed between glass wool plugs in a quartz U-tube reactor. The samples were first reduced at 500 °C for 30 min in 10% H_2/He (50 sccm) and then cooled to 100 °C under He (50 sccm). The samples were subsequently heated to 800 °C at 10 °C/min in a 10% CO_2/He flow (50 sccm).

For the four-cycle RWGS-CL experiments (looping), approximately 100 mg of the sample was placed between glass wool plugs in a quartz U-tube reactor. The sample was first heated to 500 °C in He (50 sccm). Reduction was performed in 10% H_2/He (50 sccm, 30 min), followed by oxidation in 10% CO_2/He (50 sccm, 30 min). Each reduction-oxidation sequence constituted one cycle, with four cycles conducted per material.

2.2.5. Cost and Sensitivity Analysis

To compare the economic feasibility of the ball milling method for synthesizing LCF with the conventional Pechini method, a cost analysis was performed considering the cost of the precursors, energy required, equipment needed, and process time for lab-scale (100 g) and industrial-scale (1000 kg) production of the LCF material.

Catcost v1.1.0 model [21] was used to estimate manufacturing cost. This free tool adjusts material cost estimates according to the entered production scale, which helps with early-stage cost estimations and decision-making [22]. 2021 is considered the basis

year, with losses during production (waste/spoilage) equal to 3%. The description of assumptions made, including input costs, is provided in the Supporting Information.

For each synthesis method, the sensitivity analysis was performed to understand the impact of varying a certain cost input on the net cost. This is an important step for evaluating uncertainty and for better understanding opportunities and risks, facilitating decision-making. It provides information to visualize where the process can be improved.

The sensitivity analysis was performed on raw material cost, waste losses, product mass yield, and selling margin, with a ± 30% variation in precursor cost. Sensitivity analysis was conducted using the Catcost v1.1.0 model, as described for cost analysis.

3. Results and Discussion

3.1. Structural and Morphological Properties

3.1.1. XRD Analysis

XRD analysis confirmed the formation of a cubic perovskite structure for LCF synthesized using La_2O_3, CaO, and Fe_2O_3, with no detectable secondary phases (Figure 1). The diffraction lines observed at 2θ values of 23°, 32°, 40°, 47°, 53°, 58°, 67°, and 77° are characteristic of the perovskite structure (ref. JCPDS No. 01-075-0279 [23]). The crystallite sizes, estimated using the Scherrer equation based on the main diffraction line at 2θ = 32°, are 118.9, 252.7, 336.9, and 404.3 Å for LCF-NC, LCF-800, LCF-950, and LCF-1050, respectively. These results clearly demonstrate that the crystallite size increases with rising calcination temperature. In contrast, samples synthesized using $La(NO_3)_3{\cdot}6H_2O$ and $Fe(NO_3)_3{\cdot}9H_2O$, besides the expected perovskite phases (standard $LaFeO_3$ synthesized by the Pechini method, Figure 2a, ref. JCPDS No. 37-1493 [24]), exhibited distinct peaks at 29.5° and 30.5° (La_2O_3, Figure 2b, ref. JCPDS No. 05-0602 [25]) and at 33° and 36° (Fe_2O_3, Figure 2c, ref. JCPDS No. 33-0664 [26]), indicating incomplete reaction and presence of unconverted precursors (Figure 3). This suggests that using metal oxide precursors allows more effective phase formation via ball milling, whereas nitrate-based synthesis cannot yield a pure perovskite oxide phase under the same synthesis conditions.

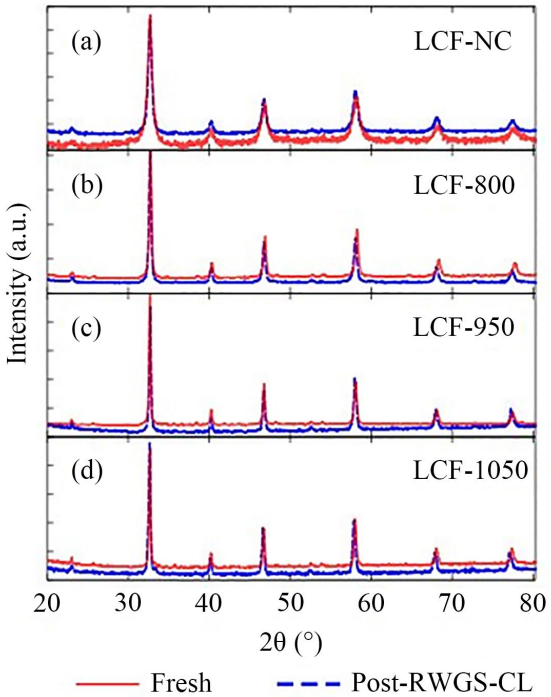


Figure 1. XRD results of ball-milling synthesized LCF using metal oxide precursors and calcined at different temperatures: (**a**) no calcination (NC), (**b**) 800 °C, (**c**) 950 °C, and (**d**) 1050 °C.

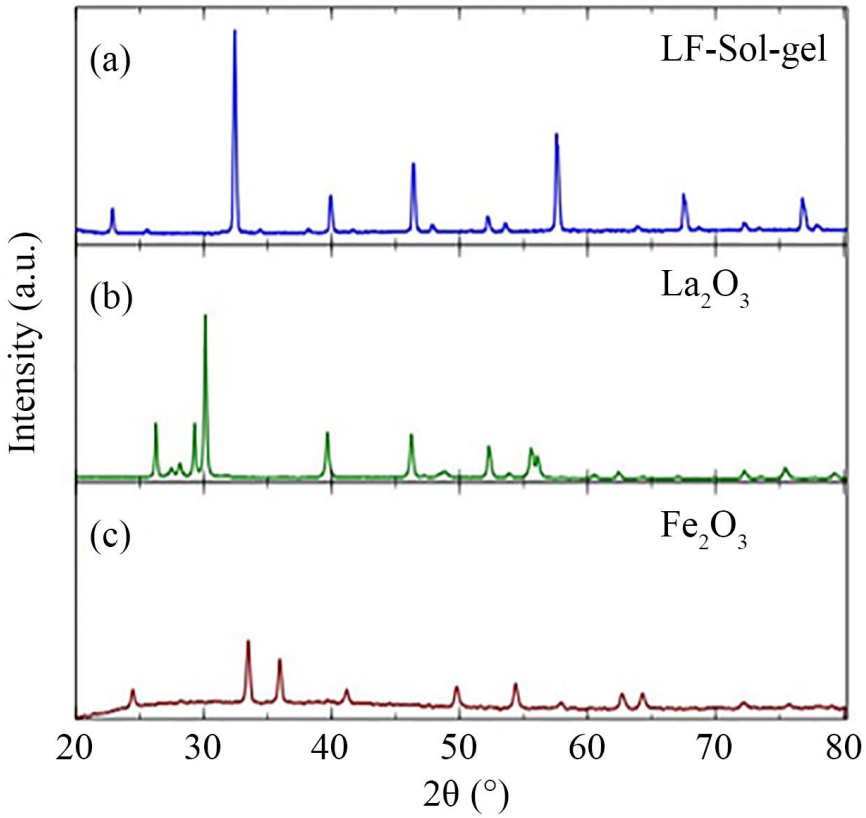


Figure 2. XRD results of referenced samples: (**a**) $LaFeO_3$ made by sol–gel; (**b**) La_2O_3 made by calcinating $La(NO_3)_3{\cdot}6H_2O$; (**c**) Fe_2O_3 made by calcinating $Fe(NO_3)_3{\cdot}9H_2O$.

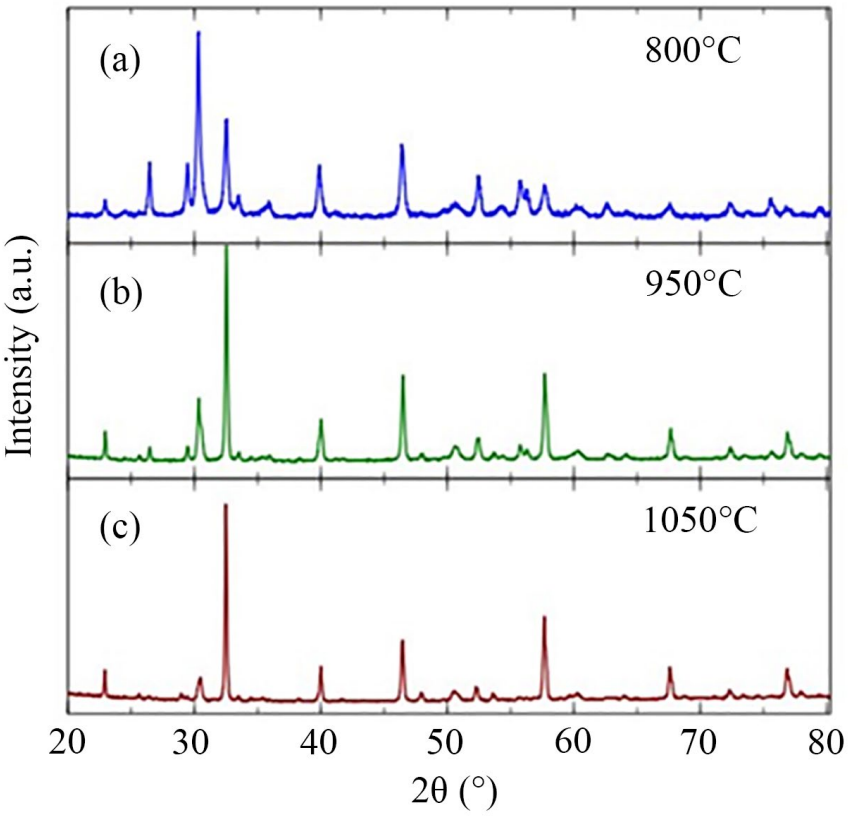


Figure 3. XRD patterns of LF synthesized by ball milling using nitrate precursors and calcined at different temperatures: (**a**) 800 °C; (**b**) 950 °C; (**c**) 1050 °C.

The crystalline phase characteristic of the perovskite structure remains unchanged in the spent materials after four cycles (Figure 1), with diffraction line intensities comparable to those of the fresh LCF. A slight shift toward lower 2θ angles is observed for several lines, and this feature was also reported in the literature [27]. Overall, these results indicate that the materials maintain structural stability without significant deactivation and could be recycled beyond the four cycles tested.

3.1.2. N_2-Physisorption Results

The BET results (Table 1) show a decreasing trend in surface area with increasing calcination temperature. The LCF-NC sample exhibits the highest surface area (2.51 m^2/g), while LCF-1050 drops to 0.51 m^2/g. The total pore volume also significantly decreases from 0.020 cm^3/g (LCF-NC) to 0.001 cm^3/g (LCF-1050), accompanied by a reduction in average pore size. These results suggest that high-temperature treatment leads to sintering and densification of the material, reducing accessible porosity [28]. Compared to LCF synthesized by the Pechini method (LCF-P), which has a surface area of 1.59 m^2/g, the ball-milled LCF-NC provides a modest improvement, though the scalability and simplicity of ball milling remain significant advantages. SEM analysis of fresh LCF-1050 revealed an average particle size of 4.23 μm, which is significantly smaller than the 196 μm observed for LCF synthesized via the Pechini method (Figures S1 and S2).

Table 1. Results of BET surface area, BJH total pore volume, and average pore diameter tested by N_2-physisorption.

Sample Name	BET Surface Area (m^2/g)	Total Pore Volume (cm^3/g)	Average Pore Diameter (nm)
La_2O_3 [a]	13.2	0.036	5.4
Fe_2O_3 [a]	12.5	0.079	12.6
CaO [a]	5.7	0.016	5.7
LCF-NC [b]	2.5	0.020	21.9
LCF-800 [b]	1.8	0.016	12.7
LCF-950 [b]	0.83	0.002	5.1
LCF-1050 [b]	0.51	0.001	4.9
LCF-P [29] [c]	1.6	N/A	N/A

[a] Oxide precursors for LCF synthesis. [b] LCF synthesized by the ball milling method with different calcination temperatures. [c] LCF from reference synthesized by the Pechini method.

3.2. Redox Properties and Oxygen Vacancy Formation

3.2.1. H_2-TPR Analysis

The temperature-programmed reduction (H_2-TPR) results (Figure 4) reveal that LCF-NC exhibits multiple reduction peaks centered at approximately 500 to 515 °C and 640 °C. This indicates different reduction phases of LCF as shown by the TPR traces. The peak at approximately 500 °C is from the formation of an oxygen vacancy, and the peak at approximately 640 °C is from the decomposition of the perovskite structure. Compared with LCF synthesized without calcination and at high calcination temperatures, the high calcination temperature leads to a modest increase in reduction temperature. These results suggest that ball milling without high-temperature treatment produces materials with slightly higher redox properties, which is beneficial for cyclic redox processes like RWGS-CL. To benchmark the redox behavior of the ball-milled LCF against materials prepared by other synthesis routes, the H_2-TPR profile was compared with the LCF synthesized by

the Pechini method [30,31]. Compared with Pechini-derived LCF reported in the literature, the ball-milled LCF exhibits comparable low-temperature redox behavior (reduction temperature of 500 to 515 °C vs. 500 °C), indicating that ball milling is an effective alternative synthesis route for producing redox-active LCF.

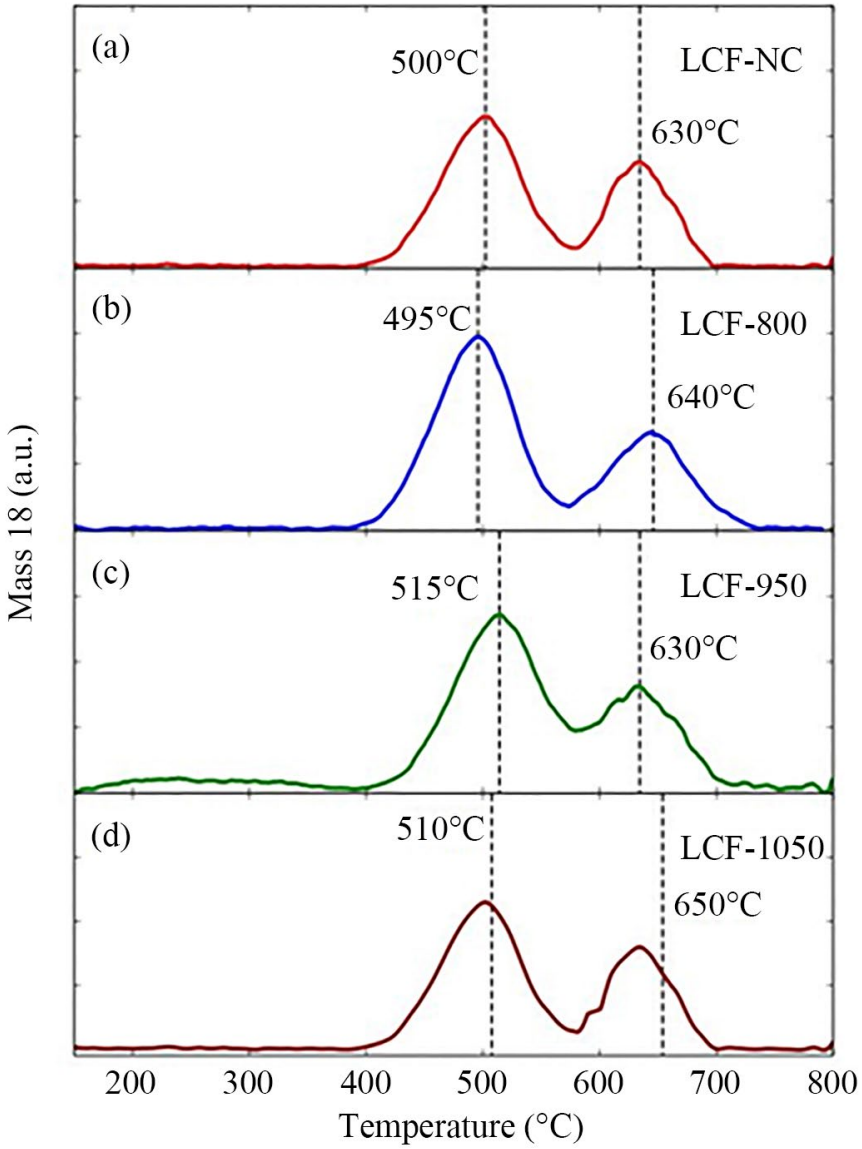


Figure 4. H_2-TPR results of LCF synthesized by the ball milling method calcined at different temperatures: (**a**) no calcination, (**b**) 800 °C, (**c**) 950 °C, and (**d**) 1050 °C.

3.2.2. CO_2 -TPO Analysis

Temperature-programmed oxidation (CO_2-TPO) experiments complemented the H_2-TPR results by delineating the reoxidation behavior. The oxidation results for the reduced LCF typically displayed a broad peak centered around 500 °C (Figure 5). This peak is attributed to the reoxidation of the oxygen-deficient sites by converting CO_2 to CO. The TPO results further suggest that reoxidation kinetics are influenced by its thermal history. The samples calcined at higher temperatures showed relatively higher oxidation temperature, indicating that the formation of a well-ordered crystalline structure requires more energy to be oxidized. Additionally, non-calcination LCF and low-temperature calcination LCF (800 °C) showed broader oxidation peaks due to the heterogeneous defect structure generated during ball milling.

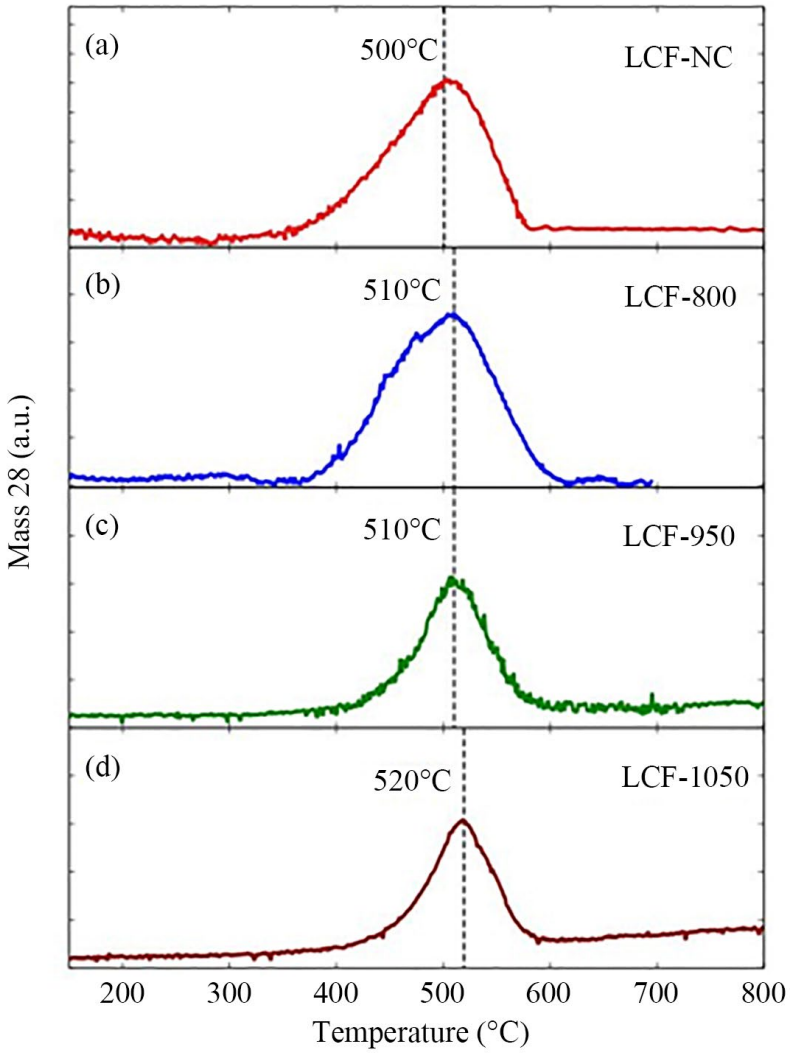


Figure 5. CO_2-TPO results of LCF synthesized by the ball milling method calcined at different temperatures: (**a**) no calcination, (**b**) 800 °C, (**c**) 950 °C, and (**d**) 1050 °C.

3.3. CO_2 Conversion and Chemical Looping Performance

The CO_2 conversion performances of ball-milled LCF samples were evaluated through four-cycle RWGS-CL at 500 °C, as shown in Figure 6. Product yields are reported as the CO signal intensity from mass spectrometry, which reflects the extent of CO formation during the oxidation step of each cycle. Prior to these 4 cycles, the first two redox cycles exhibit a large difference between H_2O and CO production due to the surface impurities, which are considered as the pretreatment cycles before activating the materials and stabilizing the redox behavior [6]. As a result, all ball-milled LCF exhibits stable CO yield (calculated by averaging the CO yield of third and fourth redox cycles) in RWGS-CL experiments, which are 910, 900, 970, and 910 μmol/g_{LCF} for LCF-NC, LCF-800, LCF-950, and LCF-1050, respectively.

The LCF-NC sample (Figure 6a), which was directly made after the ball-milling process without high-temperature calcination, exhibited the highest H_2O yield in the first cycle because there were more residues on the surface. With increased calcination temperature, the first-cycle H_2O yield decreases, because surface residues are removed by high-temperature calcination. However, even after calcination at 1050 °C, pretreatment of two redox cycles is still necessary. Then, the non-calcination LCF is considered as having the same RWGS-CL performance as high-temperature calcination LCF.

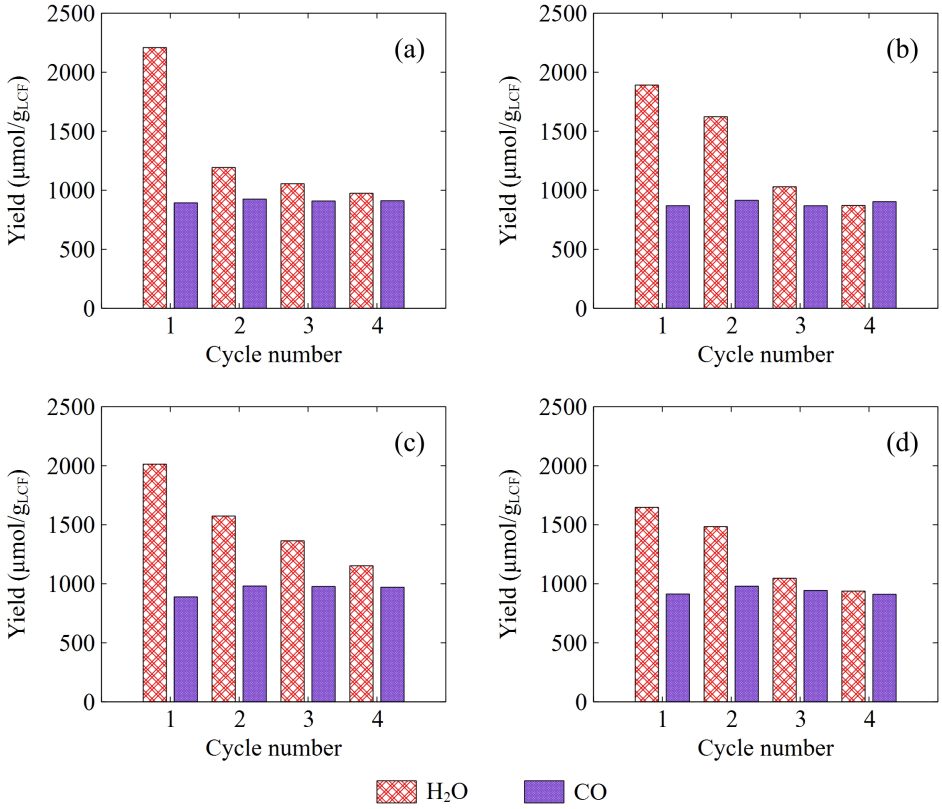


Figure 6. RWGS-CL results of LCF synthesized by the ball milling method calcined at different temperatures: (**a**) no calcination, (**b**) 800 °C, (**c**) 950 °C, and (**d**) 1050 °C.

3.4. Cost and Sensitivity Analysis

The Catcost v1.1.0 model was used to estimate the manufacturing cost. To evaluate the economic feasibility of the ball milling method for synthesizing LCF, a comparative cost analysis was performed with the conventional Pechini method. The analysis considers both precursor and process-related costs for producing LCF at lab-scale (100 g; Table 2) and industrial-scale (1000 kg; Table 3).

Ball milling utilizes relatively low-cost oxide precursors (La_2O_3, CaO, and Fe_2O_3), totaling approximately $118 for 100 g of product. In contrast, the Pechini method relies on metal nitrates and organic agents (citric acid and ethylene glycol), leading to a significantly higher precursor cost of $1432. Consider the overhead cost, the cost for LCF is $2.1/g by ball milling and $25.5/g by the Pechini method. When scaling to 1000 kg of LCF, the economic advantage of ball milling becomes even more pronounced. Bulk precursor sourcing reduces the oxide-based material cost to $32,500, compared to $274,100 for nitrate-based synthesis. As a result, the cost for LCF is $58/kg by ball milling and $487/kg by the Pechini method.

Overall, in the lab-scale (100 g) synthesis, the cost per gram of LCF synthesized by ball milling ($2.1/g) is approximately nearly 8% of that from the Pechini route ($25.5/g). On an industrial scale, the cost per kilogram of LCF synthesized by ball milling ($58/kg) is approximately nearly 12% of that from the Pechini route ($487/kg). Thus, the ball milling method significantly reduced the cost by using metal oxides instead of metal nitrates and eliminating the need for a complexing reagent. Beyond its economic advantage, ball milling also offers a simpler, solvent-free process with fewer steps and has the potential to lower the environmental impacts, especially when comparing the life cycle assessment [32] of processes using ball milling and magnetic stirring (as expected for the Pechini method), but further investigation is needed to confirm it. Due to its scalability, low cost, and ease of implementation, ball milling presents a promising synthesis route for large-scale industrial production of perovskite-type oxides. This method is especially attractive for

applications like RWGS-CL, where cost-effectiveness and material throughput are critical for commercialization.

Table 2. Cost analysis of 100g LCF synthesized by ball milling and Pechini methods.

	Ball Milling	**Pechini**
Precursors	Metal oxides	Metal nitrates and organics
Precursor and processing costs *	$118	$1432
Overheads and margin	$91	$1112
Cost per gram LCF	$2.1	$25.5

* Precursor costs are based on Sigma-Aldrich prices; details are shown in supporting information (Tables S1 and S2 [33–40]).

Table 3. Cost analysis of 1000kg LCF synthesized by ball milling and Pechini methods.

	Ball Milling	**Pechini**
Precursors	Metal oxides	Metal nitrates and organics
Precursor and processing costs *	$32,500	$274,100
Overheads and margin	$25,200	$212,500
Cost per kilogram LCF	$58	$487

* Precursor costs are based on Alibaba prices; details are shown in supporting information (Tables S3 and S4 [40–48]).

For the sensitivity analysis, the three variation levels represent the lower-case, base-case, and upper-case scenarios, respectively. This explanation clarifies why Figures 7 and 8 show a range of variations for each variable analyzed. The sensitivity analysis of LCF synthesized by ball milling (Figure 7) shows that among the selected parameters, the selling margin, the catalyst mass yield, and lanthanum precursor cost had a significant effect on the synthesized catalyst cost. The results show that the costs of iron and calcium precursors, as well as the estimated losses, do not significantly affect the net catalyst cost. The results emphasize that the catalyst cost can be reduced by increasing the catalyst mass yield to produce more than 1000 kg of catalyst, which is also expected to reduce the bulk cost of metal precursors.

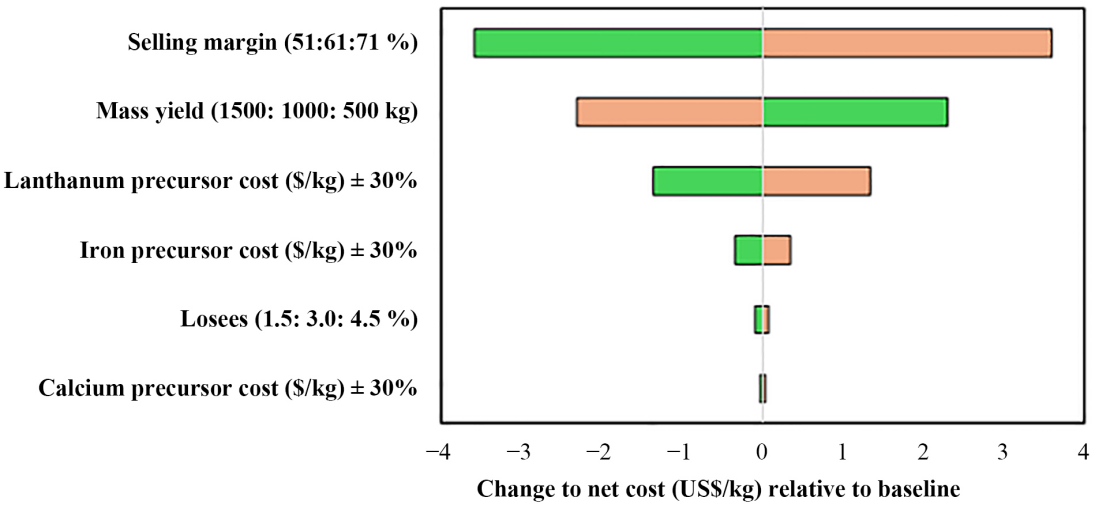


Figure 7. Sensitivity analysis for the synthesis of LCF synthesized by ball milling. Baseline catalyst cost of US$ 57.78 per kg of catalyst. 2021 is considered the basis year. The orange bar represents the high value, and the green bar represents the lower value.

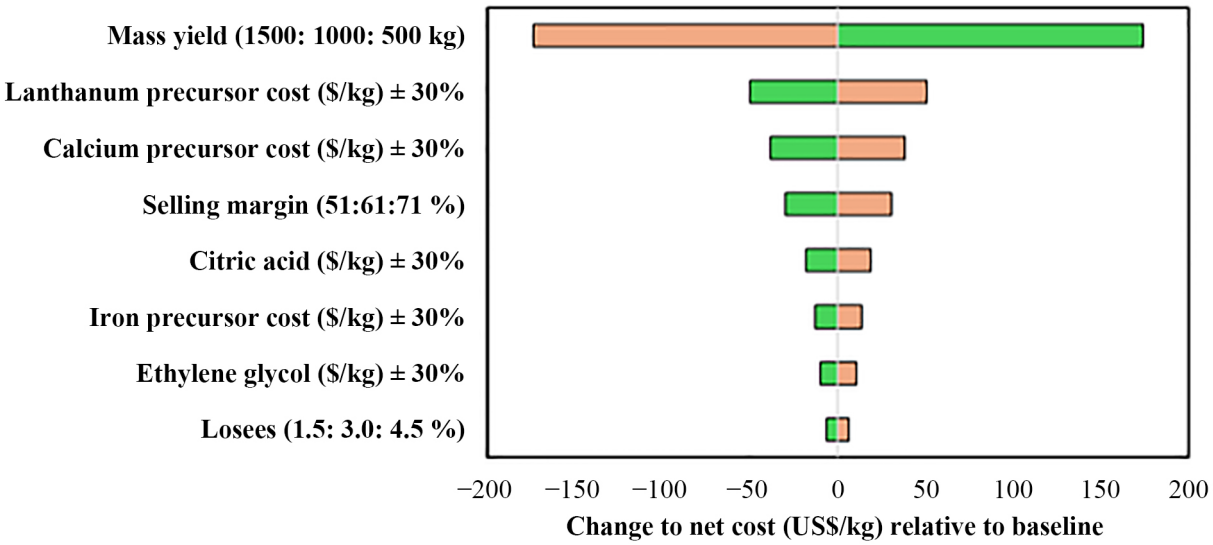


Figure 8. Sensitivity analysis for the synthesis of LCF synthesized by the Pechini method. Baseline catalyst cost of US$ 486.97 per kg of catalyst. 2021 is considered the basis year. The orange bar represents the high value, and the green bar represents the lower value.

Considering the sensitivity analysis of LCF synthesized by the Pechini method (Figure 8), it should be noted that the baseline catalyst cost ($487/kg of catalyst) is much higher than the baseline cost of LCF synthesized by ball milling ($58/kg of catalyst). The metal precursors used in the Pechini method have a higher cost than the precursors used in the ball milling method, based on the base case of producing 1000 kg. Along the same lines as discussed before, lanthanum precursor cost is the highest among the metal precursor costs.

In summary, for both synthesis methods, it can be stated that catalyst cost varies greatly with manufacturing scale, as shown in the graphical results for catalyst mass yield, with the Pechini method representing the highest net cost to produce LCF catalyst.

4. Conclusions

In this study, LCF perovskite was synthesized using a ball milling method and evaluated for CO_2-to-CO conversion via RWGS-CL. The results demonstrate that using oxide precursors (La_2O_3, CaO, and Fe_2O_3) in ball milling leads to the successful formation of a pure perovskite phase without impurities, unlike nitrate-based precursors. Structural characterization confirmed that the perovskite structure remains intact across different calcination conditions, though higher calcination temperatures reduce surface area and pore volume due to sintering.

Redox characterization showed that the non-calcined and low-temperature calcined LCF samples exhibit favorable oxygen vacancy formation and reoxidation properties, while high-temperature calcined LCF required slightly higher redox temperature. RWGS-CL experiments at 500 °C revealed that all LCF samples, regardless of post-treatment temperature, provided consistent CO yields after initial pretreatment cycles. These results proved that ball milling without calcination is a promising one-step method for the synthesis of pure LCF for converting CO_2 to CO via the RWGS-CL reaction.

A comparative cost analysis further supports the industrial relevance of the ball milling method. It showed that LCF synthesized via ball milling is significantly more cost-effective, with material costs approximately 92% lower at the lab scale and 88% lower at the industrial scale, compared to the Pechini method. Combined with its simplicity, scalability, and solvent-free nature, ball milling emerges as a promising route for large-scale production of perovskite oxides for CO_2 conversion applications.

The sensitivity analysis results for the LCF synthesis by ball milling and by the Pechini method show that the manufacturing scale has the greatest effect on the net material cost, with the Pechini method showing the highest baseline cost ($487/kg), considering 2021 the base year for calculations. Considering the metal precursors used in the synthesis, lanthanum precursors represent the biggest contribution in cost compared to the calcium and iron precursors.

Supplementary Materials: The following supporting information can be downloaded at: https://www.mdpi.com/article/10.3390/suschem7030035/s1. Figure S1: SEM results of fresh LCF synthesized by ball milling method; Figure S2: SEM results of fresh LCF synthesized by Pechini method; Table S1: Precursor cost for 100 g LCF synthesis by ball milling method; Table S2: Precursor cost for 100 g LCF synthesis by Pechini method; Table S3: Precursor cost for 1000 kg LCF synthesis by ball milling method; Table S4: Precursor cost for 1000 kg LCF synthesis by Pechini method. Table S5: Summary of CatCost parameters used for sensitivity analysis. Supporting Information is available free of charge.

Author Contributions: H.S. was the main author contributing to methodology, analysis, and writing the original draft. F.P. and H.S. contributed to the economic analysis and edited the manuscript. H.S. and P.S. contributed to the characterization techniques and to writing, revising, and editing the manuscript. V.R.B. and J.N.K. led the overall project and contributed to writing, revising, and editing the manuscript. All authors have read and agreed to the published version of the manuscript.

Funding: This study was funded by NSF grants (IIP-1743623 and IIP-1913722) and the Florida High Tech Corridor.

Institutional Review Board Statement: Not applicable.

Informed Consent Statement: Not applicable.

Data Availability Statement: The original contributions presented in this study are included in the article/Supplementary Materials. Further inquiries can be directed to the corresponding author.

Acknowledgments: The authors thank Jay Bieber and Lukasz Wojtas for technical assistance with SEM and XRD, respectively.

Conflicts of Interest: J.N.K. and V.R.B. declare patents and other financial interests in this technology. The remaining authors declare no conflicts of interest.

References

1. Daza, Y.A.; Kent, R.A.; Yung, M.M.; Kuhn, J.N. Carbon Dioxide Conversion by Reverse Water–Gas Shift Chemical Looping on Perovskite-Type Oxides. *Ind. Eng. Chem. Res.* **2014**, *53*, 5828–5837. [CrossRef]
2. Lee, M.; Kim, Y.; Lim, H.S.; Jo, A.; Kang, D.; Lee, J.W. Reverse Water–Gas Shift Chemical Looping Using a Core–Shell Structured Perovskite Oxygen Carrier. *Energies* **2020**, *13*, 5324. [CrossRef]
3. Schmidt, C.; Shi, H.; Maiti, D.; Hare, B.J.; Bhethanabotla, V.R.; Kuhn, J.N. Chemical looping approaches to decarbonization via CO_2 repurposing. *Discov. Chem. Eng.* **2023**, *3*, 15. [CrossRef]
4. Bulfin, B.; Zuber, M.; Gräub, O.; Steinfeld, A. Intensification of the reverse water–gas shift process using a countercurrent chemical looping regenerative reactor. *Chem. Eng. J.* **2023**, *461*, 141896. [CrossRef]
5. Maiti, D.; Hare, B.J.; Daza, Y.A.; Ramos, A.E.; Kuhn, J.N.; Bhethanabotla, V.R. Earth abundant perovskite oxides for low temperature CO2 conversion. *Energy Environ. Sci.* **2018**, *11*, 648–659. [CrossRef]
6. Shi, H.; Bhethanabotla, V.R.; Kuhn, J.N. Role of Ba in low temperature thermochemical conversion of carbon dioxide with $LaFeO_3$ perovskite oxides. *J. CO_2 Util.* **2021**, *51*, 101638. [CrossRef]
7. Daza, Y.A.; Maiti, D.; Hare, B.J.; Bhethanabotla, V.R.; Kuhn, J.N. More Cu, more problems: Decreased CO_2 conversion ability by Cu-doped $La_{0.75}Sr_{0.25}FeO_3$ perovskite oxides. *Surf. Sci.* **2016**, *648*, 92–99. [CrossRef]
8. Hare, B.J.; Maiti, D.; Meier, A.J.; Bhethanabotla, V.R.; Kuhn, J.N. CO_2 Conversion Performance of Perovskite Oxides Designed with Abundant Metals. *Ind. Eng. Chem. Res.* **2019**, *58*, 12551–12560. [CrossRef]
9. Shi, H.; Bhethanabotla, V.R.; Kuhn, J.N. Pelletized SiO_2-supported $La_{0.5}Ba_{0.5}FeO_3$ for conversion of CO_2 to CO by a reverse water-gas shift chemical looping process. *J. Ind. Eng. Chem.* **2023**, *118*, 44–52. [CrossRef]

10. Hare, B.J.; Maiti, D.; Daza, Y.A.; Bhethanabotla, V.R.; Kuhn, J.N. Enhanced CO_2 Conversion to CO by Silica-Supported Perovskite Oxides at Low Temperatures. *ACS Catal.* **2018**, *8*, 3021–3029. [CrossRef]
11. Feldhoff, A.; Arnold, M.; Martynczuk, J.; Gesing, T.M.; Wang, H. The sol–gel synthesis of perovskites by an EDTA/citrate complexing method involves nanoscale solid state reactions. *Solid State Sci.* **2008**, *10*, 689–701. [CrossRef]
12. Stojanovic, B.D. Mechanochemical synthesis of ceramic powders with perovskite structure. *J. Mater. Process. Technol.* **2003**, *143–144*, 78–81. [CrossRef]
13. Lee, G.-J.; Park, E.-K.; Yang, S.-A.; Park, J.-J.; Bu, S.-D.; Lee, M.-K. Rapid and direct synthesis of complex perovskite oxides through a highly energetic planetary milling. *Sci. Rep.* **2017**, *7*, 46241. [CrossRef] [PubMed]
14. Kumar, A.; Dutta, S.; Kim, S.; Kwon, T.; Patil, S.S.; Kumari, N.; Jeevanandham, S.; Lee, I.S. Solid-State Reaction Synthesis of Nanoscale Materials: Strategies and Applications. *Chem. Rev.* **2022**, *122*, 12748–12863. [CrossRef] [PubMed]
15. Webber, K.G.; Clemens, O.; Buscaglia, V.; Malič, B.; Bordia, R.K.; Fey, T.; Eckstein, U. Review of the opportunities and limitations for powder-based high-throughput solid-state processing of advanced functional ceramics. *J. Eur. Ceram. Soc.* **2024**, *44*, 116780. [CrossRef]
16. Navas, D.; Fuentes, S.; Castro-Alvarez, A.; Chavez-Angel, E. Review on Sol-Gel Synthesis of Perovskite and Oxide Nanomaterials. *Gels* **2021**, *7*, 275. [CrossRef] [PubMed]
17. Huízar-Félix, A.M.; Hernández, T.; de la Parra, S.; Ibarra, J.; Kharisov, B. Sol–gel based Pechini method synthesis and characterization of $Sm_{1-x}CaxFeO_3$ perovskite $0.1 \leq x \leq 0.5$. *Powder Technol.* **2012**, *229*, 290–293. [CrossRef]
18. Popa, M.; Kakihana, M. Synthesis of lanthanum cobaltite ($LaCoO_3$) by the polymerizable complex route. *Solid State Ion.* **2002**, *151*, 251–257. [CrossRef]
19. Calderón Bedoya, P.A.; Botta, P.M.; Bercoff, P.G.; Fanovich, M.A. Influence of the milling materials on the mechanochemical synthesis of magnetic iron oxide nanoparticles. *J. Alloys Compd.* **2023**, *939*, 168720. [CrossRef]
20. Xue, S.; Mao, H.; Li, J.; Sun, X.; Gong, Z.; Fan, B.; Shao, G.; Wang, H.; Xu, H.; Zhang, R.; et al. One-step synthesis of all-inorganic high-entropy dual-phase $Cs'B'Br_3/Cs'B'_2Br_5$ perovskite nanocrystals by high-energy ball milling. *Ceram. Int.* **2023**, *49*, 35202–35212. [CrossRef]
21. Van Allsburg, K.M.; Tan, E.C.D.; Super, J.D.; Schaidle, J.A.; Baddour, F.G. Early-stage evaluation of catalyst manufacturing cost and environmental impact using CatCost. *Nat. Catal.* **2022**, *5*, 342–353. [CrossRef]
22. Anekwe, I.M.S.; Lora, E.E.S.; Subramanian, K.A.; Kozlov, A.; Zhang, S.; Oboirien, B.; Isa, Y.M. Techno-economic and life-cycle analysis of single-step catalytic conversion of bioethanol to fuel blendstocks over Ni-doped HZSM-5 zeolite catalyst. *Energy Convers. Manag. X* **2024**, *22*, 100529. [CrossRef]
23. Zhang, L.; Zeng, Y.; Li, H.; Su, H.; Zhang, W.; Zheng, H.; Wen, N.; Huang, X.; Long, J. Engineering B-Site Configurational Entropy in Perovskite Oxides for Enhanced Alkaline Oxygen Evolution Reaction. *ChemSusChem* **2026**, *19*, e70498. [CrossRef] [PubMed]
24. Liu, Q.; You, Z.; Zeng, S.J.; Guo, H. Infrared properties of Mg-doped $LaFeO_3$ prepared by sol–gel method. *J. Sol.-Gel Sci. Technol.* **2016**, *80*, 860–866. [CrossRef]
25. Lin, N.; Wang, R.; Yu, W.; Wang, M.; Xu, Y. Up-Conversion Luminescence Enhancement and Temperature Sensitivity Properties of La_2O_3: Yb^{3+}/Er^{3+} Nanoparticles Induced via Tri-Doping Li^+ Ions. *ChemistrySelect* **2021**, *6*, 7213–7222. [CrossRef]
26. Liu, L.; Fu, S.; Lv, X.; Yue, L.; Fan, L.; Yu, H.; Gao, X.; Zhu, W.; Zhang, W.; Li, X.; et al. A Gas Sensor With Fe_2O_3 Nanospheres Based on Trimethylamine Detection for the Rapid Assessment of Spoilage Degree in Fish. *Front. Bioeng. Biotechnol.* **2020**, *8*, 567584. [CrossRef] [PubMed]
27. Daza, Y.A.; Maiti, D.; Kent, R.A.; Bhethanabotla, V.R.; Kuhn, J.N. Isothermal reverse water gas shift chemical looping on $La_{0.75}Sr_{0.25}Co_{(1-Y)}Fe_YO_3$ perovskite-type oxides. *Catal. Today* **2015**, *258*, 691–698. [CrossRef]
28. Han, R.; Wang, Y.; Xing, S.; Pang, C.; Hao, Y.; Song, C.; Liu, Q. Progress in reducing calcination reaction temperature of Calcium-Looping CO_2 capture technology: A critical review. *Chem. Eng. J.* **2022**, *450*, 137952. [CrossRef]
29. Bidrawn, F.; Lee, S.; Vohs, J.; Gorte, R. The Effect of Ca, Sr, and Ba Doping on the Ionic Conductivity and Cathode Performance of $LaFeO_3$. *J. Electrochem. Soc.* **2008**, *155*, B660–B665. [CrossRef]
30. Lim, H.S.; Lee, M.; Kang, D.; Lee, J.W. Role of transition metal in perovskites for enhancing selectivity of methane to syngas. *Int. J. Hydrogen Energy* **2018**, *43*, 20580–20590. [CrossRef]
31. Oh, D.; Colombo, F.; Nodari, L.; Kim, J.H.; Kim, J.K.; Lee, S.; Kim, S.; Kim, S.; Lim, D.-K.; Seo, J.; et al. Rocking chair-like movement of ex-solved nanoparticles on the Ni-Co doped $La_{0.6}Ca_{0.4}FeO_{3-\delta}$ oxygen carrier during chemical looping reforming coupled with CO_2 splitting. *Appl. Catal. B Environ.* **2023**, *332*, 122745. [CrossRef]
32. Yang, N.; Sheng, X.; Ti, L.; Jia, H.; Ping, Q.; Li, N. Ball-milling transesterification process on biodiesel production: RSM optimization, life cycle assessment and market dynamics analysis. *Energy* **2023**, *283*, 129201. [CrossRef]
33. Lanthanum(III) Oxide. Available online: https://www.sigmaaldrich.com/US/en/product/aldrich/l4000?utm_source=google&utm_medium=cpc&utm_campaign=22099353999&utm_content=&gad_source=1&gad_campaignid=22109359894&gbraid=0AAAAD8kLQQ97LE0Z4hhMIwmKk1kaWiSk&gclid=Cj0KCQjwjo7DBhCrARIsACWauSk264dhsWS1GN0J8FMGkiDK09xpJYriyTg27V-UC0_0lSHXK9mfCKIaAknFEALw_wcB (accessed on 17 December 2025).

34. Calcium Oxide. Available online: https://www.sigmaaldrich.com/US/en/substance/calciumoxide56081305788 (accessed on 17 December 2025).
35. Iron(III) Oxide. Available online: https://www.sigmaaldrich.com/US/en/substance/ironiiioxide159691309371 (accessed on 13 December 2025).
36. Lanthanum(III) Nitrate Hexahydrate. Available online: https://www.sigmaaldrich.com/US/en/search/la(no3)3?focus=products&page=1&perpage=30&sort=relevance&term=la(NO3)3&type=product (accessed on 17 December 2025).
37. Calcium Nitrate Tetrahydrate. Available online: https://www.sigmaaldrich.com/US/en/search/cano3?focus=products&page=1&perpage=30&sort=relevance&term=CaNO3&type=product (accessed on 17 December 2025).
38. Iron(III) Nitrate Nonahydrate. Available online: https://www.sigmaaldrich.com/US/en/search/fe(no3)3?focus=products&page=1&perpage=30&sort=relevance&term=Fe(NO3)3&type=product (accessed on 8 December 2025).
39. Citric Acid. Available online: https://www.sigmaaldrich.com/US/en/search/citric-acid?focus=products&page=1&perpage=30&sort=relevance&term=Citric%20acid&type=product (accessed on 10 December 2025).
40. Ethylene Glycol. Available online: https://www.sigmaaldrich.com/US/en/search/ethylene-glycol?focus=products&page=1&perpage=30&sort=relevance&term=Ethylene%20glycol&type=product(accessed on 12 December 2025).
41. High Quality 99.99% Pure Lanthanum Oxide (La_2O_3) Excellent Chemical Additive Materials Good Price. Available online: https://www.alibaba.com/product-detail/High-Pure-Lanthanum-Oxide-99-99_10000023532715.html?spm=a2700.7724857.0.0.485670e2V93Gvy (accessed on 10 December 2025).
42. High Quality Calcium Oxide Quick Lime Purity 95% Best Brand Supplier Price. Available online: https://hongyu8888.en.made-in-china.com/product/enqRplrJqjkG/China-High-Quality-Calcium-Oxide-Quick-Lime-Purity-95-Best-Brand-Supplier-Price.html?pv_id=1j2qamvb8e0d&faw_id=1j2qar4nu95d&bv_id=1j2qar4o4f83&pbv_id=1j2qamu56ec5m (accessed on 8 December 2025).
43. Iron Oxide Red for Chemical Fertilizer for Cement for Concrete Flooring Powder Blue for Epoxy Floor Paint 99% Nano Micron Size. Available online: https://www.alibaba.com/product-detail/iron-oxide-red-for-chemical-fertilizer_1601259481418.html?spm=a2700.7724857.0.0.704538f0wHhW23 (accessed on 10 December 2025).
44. Factory Supply Lanthanum(III) Nitrate Hexahydrate with $La(NO_3)_3$ CAS 10277-43-7 Lanthanum Nitrate With Nice Price. Available online: https://www.alibaba.com/product-detail/Factory-Supply-Lanthanum-III-Nitrate-Hexahydrate_1601014444011.html?spm=a2700.galleryofferlist.normal_offer.d_title.69a013a0RM9ayL (accessed on 10 December 2025).
45. Calcium Threonate Powder Food Grade CAS 70753-61-6 Assay 99% C8H14CaO10 Calcium L-Threonate. Available online: https://www.alibaba.com/product-detail/Calcium-Threonate-Powder-Food-Grade-CAS_1600991474732.html?spm=a2700.galleryofferlist.normal_offer.d_title.561713a0CS91Tw (accessed on 10 December 2025).
46. 99% Ferric Nitrate Price Iron Nitrate Nonahydrate. Available online: https://www.alibaba.com/product-detail/99-Ferric-Nitrate-Price-Iron-Nitrate_1600820644048.html?spm=a2700.galleryofferlist.normal_offer.d_title.332513a0tC8uXk (accessed on 10 December 2025).
47. 99.5% Purity Food Grade ENSIGN TTAC LEMON STAR Citric Acid Monohydrate Anhydrous Competitive Price Food Additive. Available online: https://www.alibaba.com/product-detail/99-5-Purity-Food-Grade-ENSIGN_1601367646934.html?spm=a2700.galleryofferlist.normal_offer.d_title.31c613a0aaaQvp&priceId=31800ee795da4c00913daf1ffe547a29 (accessed on 10 December 2025).
48. Factory Supply 99.9% MEG Monoethylene Glycol Ethylene Glycol Ethylene Glycol Liquid. Available online: https://www.alibaba.com/product-detail/Factory-Supply-99-9-MEG-Monoethylene_1601523642161.html?spm=a2700.galleryofferlist.normal_offer.d_title.5d3213a0fozDok&priceId=9cf109372bc9456589e59dd2bb18170f (accessed on 10 December 2025).

Disclaimer/Publisher's Note: The statements, opinions and data contained in all publications are solely those of the individual author(s) and contributor(s) and not of MDPI and/or the editor(s). MDPI and/or the editor(s) disclaim responsibility for any injury to people or property resulting from any ideas, methods, instructions or products referred to in the content.